Kinetics of desolvation of inclusion compounds of 9,10-derivatives of *trans*-9,10-dihydroxy-9,10-dihydroanthracene with benzene †

Leonard J. Barbour,[a] Mino R. Caira,[b] Anita Coetzee*,[b] and Luigi R. Nassimbeni[b]
[a] *Department of Chemistry, University of Missouri-Columbia, 123 Chemistry Building, Columbia, Missouri 65211, USA*
[b] *Department of Chemistry, University of Cape Town, Rondebosch 7700, South Africa*

The structures of the inclusion compounds of *trans*-9,10-dihydroxy-9,10-di-*p*-*tert*-butylphenyl-9,10-dihydroanthracene (DDTBDA) and *trans*-9,10-dihydroxy-9,10-di-α-naphthyl-9,10-dihydroanthracene (DDNDA) with benzene, with host:guest ratios of 1:3 and 1:1, respectively, have been elucidated. Their isothermal kinetics of desolvation have been studied. DDTBDA·3benzene desolvates in a single deceleratory step following the first-order kinetic model. The α *vs.* time curves for the desolvation of DDNDA·benzene are of truncated sigmoidal shape and are best described by the Prout–Tomkins model.

The host compound *trans*-9,10-dihydroxy-9,10-diphenyl-9,10-dihydroanthracene and its inclusion compounds with a variety of guests have been studied extensively. The structure of the non-porous α-phase,[2] as well as those of its inclusion compounds with a number of aliphatic[3–6] and aromatic[7] guests, have been elucidated.

The thermal decomposition of the inclusion compound with acetonitrile has been investigated[8] using the method of Flynn and Wall,[9] which yielded an approximate value of the activation energy of the desolvation process. We have recently investigated the kinetics of enclathration of acetone by this host, and shown that it exhibits anti-Arrhenius kinetics.[10]

Thermal decomposition of organic inclusion compounds has not received a great deal of attention. This may be due to the fact that the decomposition often involves multiple steps, with the formation of new intermediate host–guest phases whose composition and structure are not readily established. We have studied the thermal desolvation of the inclusion compounds of 2,2′-bis(2,7-dichloro-9-hydroxy-9-fluorenyl)biphenyl with 1,4-dioxane and 1,3-dioxolane.[11] The kinetics were analysed by isothermal decomposition runs at selected temperatures and curve fitting techniques allowed us to select suitable models to describe the desolvation mechanism and derive the appropriate Arrhenius parameters.

We now present the results of the structures and thermal desolvation of two tricyclic host compounds, *trans*-9,10-dihydroxy-9,10-di-*p*-*tert*-butylphenyl-9,10-dihydroanthracene and *trans*-9,10-dihydroxy-9,10-di-α-naphthyl-9,10-dihydroanthracene, which form inclusion compounds with benzene (see Scheme 1). These host compounds are directly related to the parent *trans*-9,10-dihydroxy-9,10-diphenyl-9,10-dihydroanthracene.

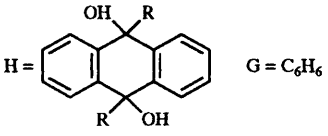

H : G

1 R = *p*-*tert*-butylphenyl 1 : 3

2 R = α-naphthyl 1 : 1

Scheme 1

Experimental

The inclusion compounds were obtained by dissolving the appropriate host compounds in an excess of benzene. Crystals of diffraction quality were obtained by slow evaporation of the solutions. X-ray diffraction data were measured on an Enraf-Nonius CAD4 diffractometer, using graphite-monochromated Mo-Kα radiation (λ = 0.7107 Å) and the ω–2θ scan mode. The selected crystals were sealed in Lindemann capillary tubes together with mother liquor in order to prevent desorption of the guest. During data collection three reference reflections were monitored periodically to check crystal stability. The data reduction included correction for Lorentz and polarisation effects. A linear decay correction was applied to the data set of compound **1**, which showed an overall loss in intensity of 14.3%. Crystal data and structural refinement parameters are given in Table 1.

Differential scanning calorimetry (DSC) and thermal gravimetry (TG) were performed on a Perkin-Elmer PC7 series system. Finely powdered specimens, obtained from continuously stirred solutions, were blotted dry on filter paper and placed in open platinum pans for TG experiments and in crimped, but vented aluminium sample pans for DSC experiments. The sample weight in each case was 2–5 mg. The temperature range was typically 30–300 °C at a heating rate of 20 °C min^{-1}. The samples were purged by a stream of nitrogen flowing at 40 cm^3 min^{-1}. Data for the kinetics of desolvation were obtained from isothermal TG experiments carried out at selected temperatures in the range 50–70 °C for compound **1** and 70–85 °C, for compound **2**.

Results and discussion

Structure solution and refinement

The structures were solved by direct methods using SHELX-86[12] and refined by full-matrix least-squares methods on F, with SHELX-76.[13] Direct methods yielded all the non-hydrogen atoms in the asymmetric unit. In each case the hydroxy hydrogen atoms were located in the difference electron density maps and refined with bond length constraints[14] and individual temperature factors. The rest of the hydrogen atoms were placed with geometric constraints and refined with a common isotropic temperature factor.

For compound **1**, TG yielded a host:guest ratio of 1:3. Since it crystallises in the space group $P2_1/c$ with Z = 2, this requires

† Complexation with diol host compounds, Part 22. For part 21, see ref. 1.

Table 1 Crystal data and refinement parameters

Crystal data	1	2
Molecular formula	$C_{34}H_{36}O_2 \cdot 3(C_6H_6)$	$C_{34}H_{24}O_2 \cdot C_6H_6$
M_r	711.00	542.68
Space group	$P2_1/c$	$P\bar{1}$
Z	2	1
a/Å	8.970(4)	7.254(2)
b/Å	17.128(2)	9.003(3)
c/Å	13.275(2)	11.882(3)
α/°	90	108.13(2)
β/°	90.26(2)	97.40(2)
γ/°	90	101.29(2)
Volume/Å^3	2040(1)	708.0(3)
D_m/g cm^{-3}	1.15(1)	1.27(1)
D_c/g cm^{-3}	1.157	1.273
μ(Mo-Kα)/cm^{-1}	0.64	0.72
F(000)	764	286
Data collection parameters		
Crystal dimensions/mm	0.44 × 0.41 × 0.34	0.22 × 0.22 × 0.31
θ range scanned/°	1–25	1–25
Range of indices h,k,l	±10,20,15	±8, ±10,14
Total exposure time/h	26.0	18.1
Overall intensity variation (%)	−14.3	−0.2
Scan width, x in (x + 1.05 tan θ)°	0.85	0.85
No. unique reflections collected	2883	2186
No. observed reflections with $I_{rel} > 2\sigma I_{rel}$	2040	1771
Final refinement parameters		
No. variables	264	196
R	0.097	0.050
R_w	0.108	0.064
g in $w = [\sigma^2(F_o) + gF_o^2]^{-1}$	0.0027	0.05
Max. shift/esd	0.158	0.015
Avg. shift/esd	0.013	0.002
Max., min. heights in difference Fourier/e Å^{-3}	0.36, −0.34	0.20, −0.27

the host molecules to be situated at special positions with the asymmetric unit consisting of half of a host molecule and one and a half guest molecules. The structure of the host molecule with atomic labelling is shown in Fig. 1, while a projection of the structure viewed along [100] is shown in Fig. 2. The guest molecules are situated in cross-linked channels running along [011] and [01−1] in the (100) plane. This is illustrated in Fig. 3, in which the hatched area represents space occupied by the host, while the guest molecules are represented with van der Waals radii.

For compound **2**, which crystallises in the space group $P\bar{1}$ with $Z = 1$, both host and guest molecules lie at centres of inversion. The conformation of the host molecule, with atomic labelling, is shown in Fig. 4 and a projection of the structure viewed along [001] shows the benzene guests to be located in cavities, centred on the Wyckoff position g, as shown in Fig. 5.

Kinetics of desolvation

The thermal analytical results are shown in Fig. 6(*a*) and (*b*). For compound **1** the guest loss reaction takes place in a single step, with an onset temperature of 78 °C, corresponding to the loss of three benzene molecules per molecule of host. The DSC trace shows two diffuse endotherms, corresponding to overlapping thermal events. A sharp endotherm at 260 °C corresponds to the host melt which is accompanied by sublimation. The host : guest ratio of 1 : 1 for compound **2**, was confirmed by the TG experiment, showing a single mass loss step of 14.4% at an onset of 90 °C. This corresponds to a single

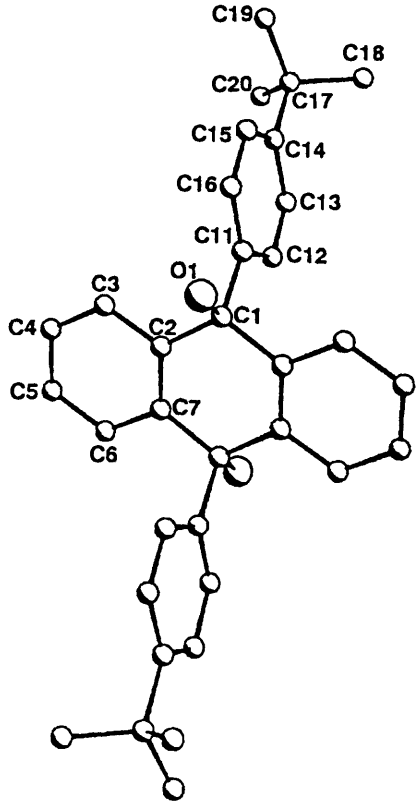

Fig. 1 Host conformation of compound **1**

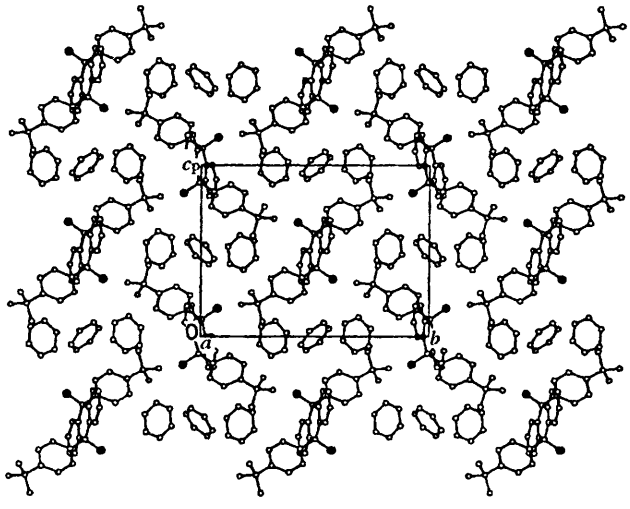

Fig. 2 Crystal packing in compound **1** as viewed down [100]

endotherm in the DSC trace, followed by the host melt at 300 °C.

A series of mass loss *vs.* time curves were obtained for the isothermal desolvation of compound **1**. The data were reduced to fractional reaction (α) *vs.* time curves. An example of an α *vs.* time curve obtained is shown in Fig. 7 and it is clearly deceleratory. Various appropriate kinetic models [15] were fitted to the data. The first-order (F1) reaction mechanism fitted this reaction over an α range of 0.1 to 0.9. The semilogarithmic plot of ln k *vs.* $1/T$ is shown in Fig. 8, which yields an activation energy of 87 (2) kJ mol^{-1}. We repeated the kinetic analysis, using rising temperature TG results, obtained at a constant heating rate of 20 °C min^{-1}. The rising temperature thermogram was converted

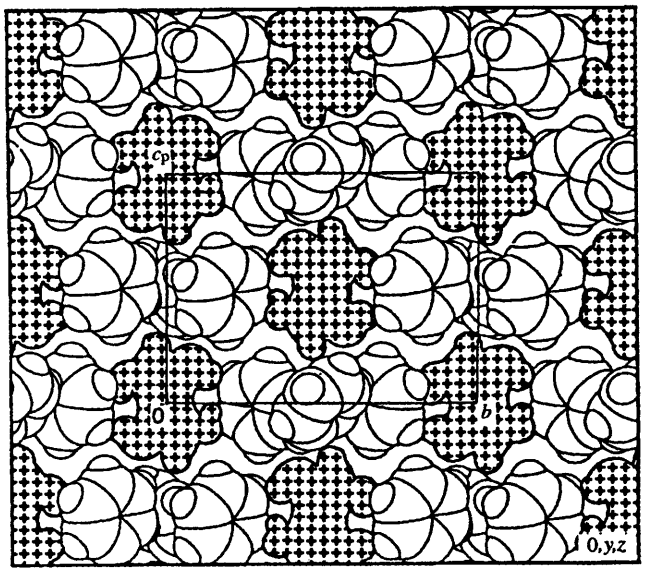

Fig. 3 Projected cross-section of the host molecules (hatched area) of compound **1** on (100) showing the guest molecules in channels

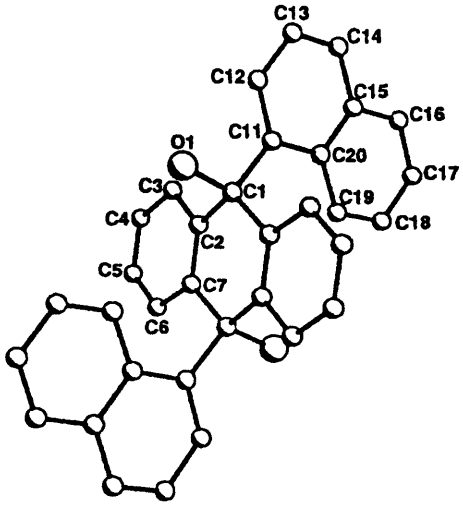

Fig. 4 Host conformation of compound **2**

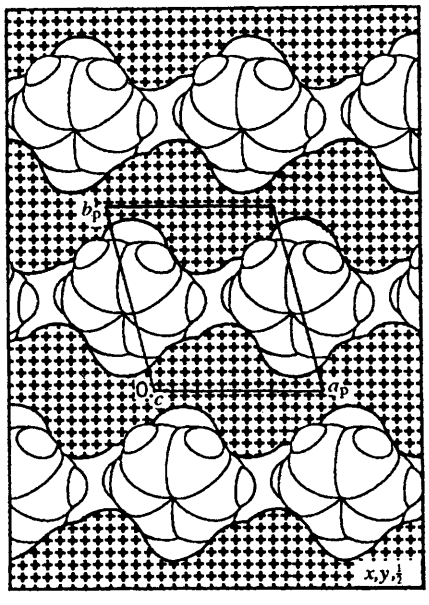

Fig. 5 Projected cross-section of the host molecules (hatched area) of compound **2** viewed along [001] on (002) showing the guest molecules in cavities

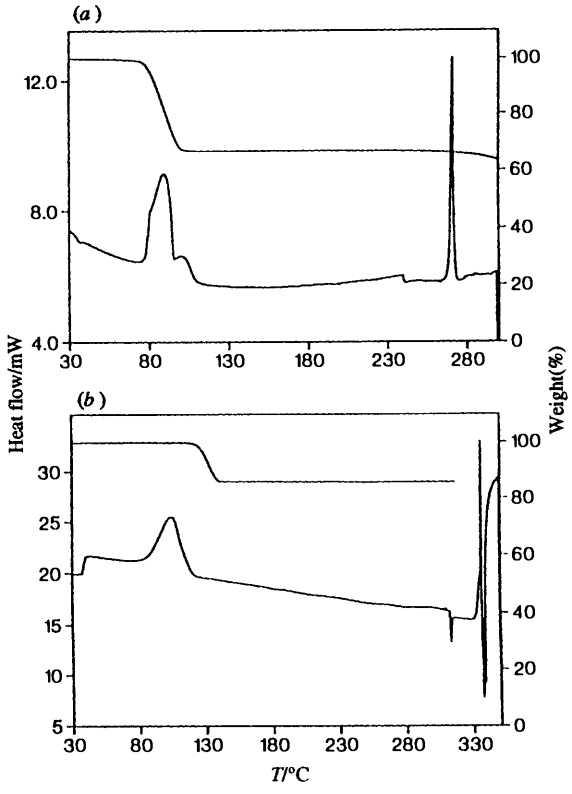

Fig. 6 Thermograms showing the desolvation of compound **1** (*a*) and compound **2** (*b*)

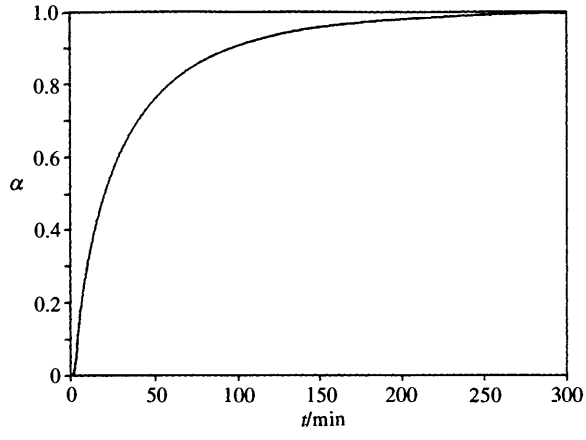

Fig. 7 Example of an isothermal α *vs.* time curve obtained for compound **1**

to an α *vs.* temperature curve. According to Borchardt and Daniels[16] $k = (d\alpha/dT)/(1-\alpha)^n$, where n is the order of the reaction. We substituted $n = 1$, from the isothermal results, and obtained a linear plot of $\ln k$ *vs.* $1/T$ over an α range of 0 to 0.58. The slope of this curve was used to calculated E_a. The intercept gave $\ln(A/\varphi)$, where φ is the constant heating rate. An activation energy of 89 (4) kJ mol^{-1} was obtained. This corresponds well with that obtained from the isothermal experiments.

An example of the α *vs.* time curves, obtained from a series of isothermal TG experiments carried out on compound **2** over a temperature range of 70–85 °C can be seen in Fig. 9. Slight irregularities were observed in the first part of the curve as the isothermal temperatures were approached. These sections were ignored in the kinetic analysis, since they occurred over a very small time period. The curves were of truncated sigmoidal shape. They did not possess a significant induction period, but clearly consisted of an acceleratory and decleratory section.

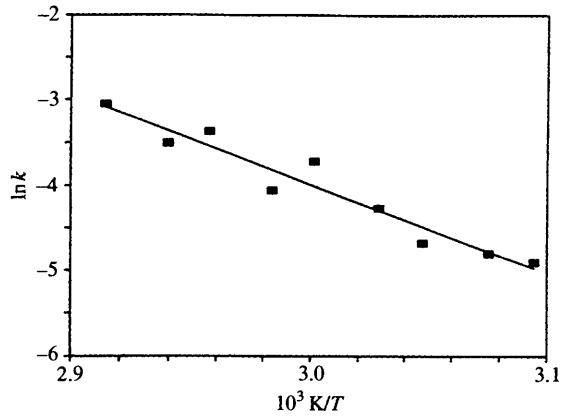

Fig. 8 Arrhenius plot for the desolvation of compound **1**

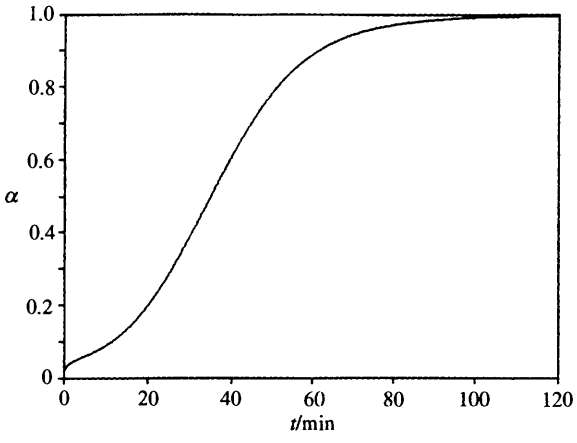

Fig. 9 Example of an isothermal α *vs.* time curve obtained for compound **2**

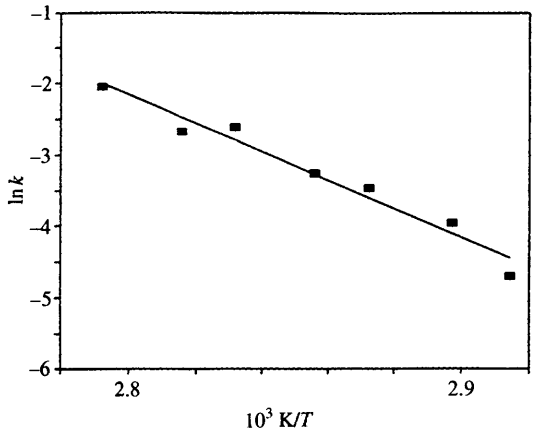

Fig. 10 Arrhenius plot for the desolvation of compound **2**

Sigmoidal kinetic models were fitted to the data and were best described by the Prout–Tomkins kinetic model. An activation energy of 116 (4) kJ mol^{-1} was obtained for this reaction over an α range of 0.05 to 0.95. A curve of ln *k* *vs.* $1/T$ is shown in Fig. 10.

X-Ray powder diffraction

X-Ray powder diffraction data were collected for the inclusion compounds as well as the desolvation products in each case. The powder patterns for the host–guest inclusion compounds and their desolvation products are shown in Fig. 11(*a*) and (*b*) for compounds **1** and **2** respectively. Each compound desolvates to form a non-porous α-phase. It is clear from the diffraction patterns that desolvation is accompanied by a phase change in each case.

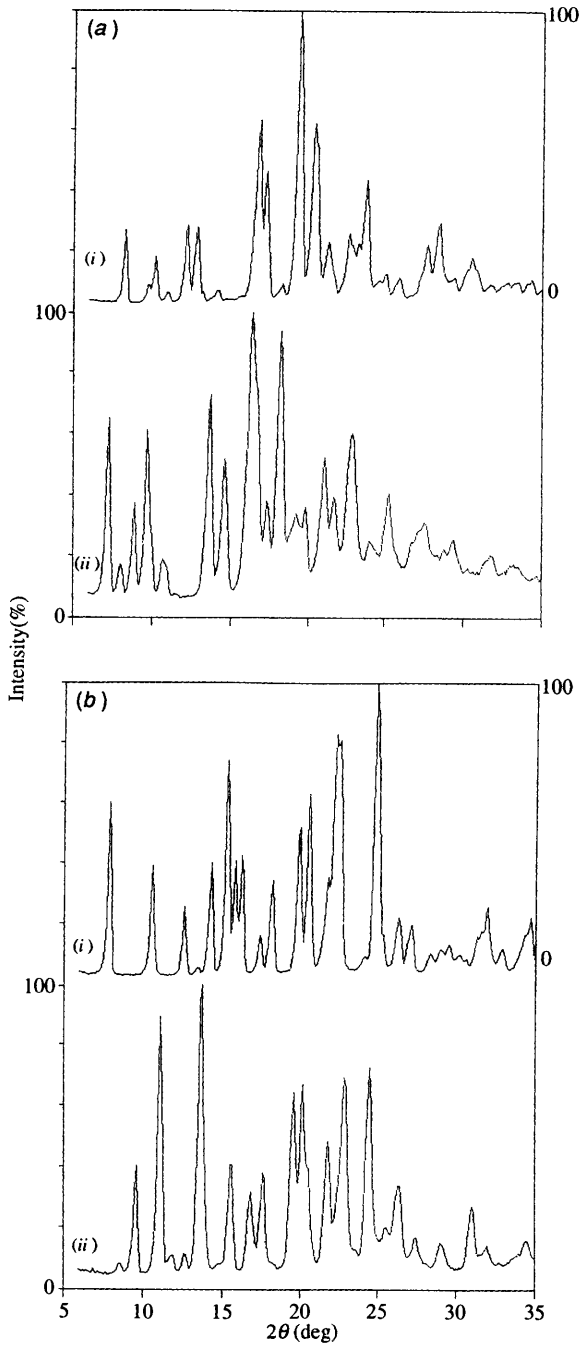

Fig. 11 (*a*) X-Ray powder diffraction traces of compound **1** (*i*) before desolvation; (*ii*) after complete desolvation (*i.e.* α-phase). (*b*) X-Ray powder diffraction traces of compound **2** (*i*) before desolvation; (*ii*) after complete desolvation (*i.e.* α-phase).

Conclusions

A typical sigmoidal curve can be divided into an induction period, an acceleratory stage and a deceleratory stage. The α *vs.* time curves for the desolvation of compound **2** lack the induction period and they can be described as truncated sigmoidal curves. The initial rate of reaction is slow and can probably be ascribed to the fact that the gaseous desolvation product cannot easily escape without disruption of the crystal structure, since the guest is captured in cavities in the host framework. The rate of reaction increases until a point of inflection is reached after which the curves become deceleratory.

The channel structure of compound **1** on the other hand would imply that the gaseous decomposition product can easily escape and does not impair the rate of the reaction. The desolvation is deceleratory and follows the F1 mechanism. The ease with which the gaseous product can escape during desolvation of compound **1**, probably explains why the activation energy for this reaction is much less than that of the desolvation of compound **2**. In both cases desolvation is accompanied by the collapse of the host crystalline phase to the non-porous α-phase. We note that the kinetic mechanisms proposed only deal with the guest loss as the rate determining step, since thermogravimetry only measures the mass loss and does not account for concomitant thermal events. Thus we cannot detail the mechanism of the phase change in the crystal structure of the host which has been shown to occur upon guest loss.

Acknowledgements

We thank the Foundation for Research Development and the University of Cape Town for financial support.

References

1 M. R. Caira, A. Horne, L. R. Nassimbeni, K. Okuda and F. Toda, *J. Chem. Soc., Perkin Trans. 2*, 1995, 1063.
2 F. Toda, K. Tanaka, S. Nagamatsu and T. C. W. Mak, *Isr. J. Chem.*, 1985, **25**, 346.
3 F. Toda, K. Tanaka, S. Nagamatsu and T. C. W. Mak, *J. Incl. Phenom.*, 1985, **3**, 225.
4 F. Toda. K. Tanaka, S. Nagamatsu and T. C. W. Mak, *Tetrahedron Lett.*, 1984, **25**, 13 359.
5 D. R. Bond, L. R. Nassimbeni and F. Toda, *J. Incl. Phenom. Mol. Recognit. Chem.*, 1989, **7**, 623.
6 D. R. Bond, L. R. Nassimbeni and F. Toda, *J. Cryst. Spectrosc. Res.*, 1989, **19**, 847.
7 D. R. Bond, M. R. Caira, G. A. Harvey, L. R. Nassimbeni and F. Toda, *Acta Crystallogr. Sect. B*, 1990, **46**, 771.
8 M. R. Caira, L. R. Nassimbeni, W.-D. Schubert and F. Toda, *Thermochimica Acta*, 1992, **206**, 265.
9 J. H. Flynn and L. A. Wall, *Polym. Lett.*, 1966, **4**, 323.
10 L. J. Barbour, M. R. Caira and L. R. Nassimbeni, *J. Chem. Soc., Perkin Trans. 2*, 1993, 2321.
11 M. R. Caira, A. Coetzee, L. R. Nassimbeni, E. Weber and A. Wierig, *J. Chem. Soc., Perkin Trans. 2*, 1995, 281.
12 G. M. Sheldrick, SHELX-86, *Crystallographic Computing 3*, eds. G. M. Sheldrick, C. Kruger and R. Goddard, Oxford University Press, 1985, p. 175.
13 G. M. Sheldrick, SHELX-76, *Computing in Crystallography*, eds. H. Schenk, Olthof-Hazekamp, J. von Koningsveld and G. C. Bassi, Delft University Press, 34, 1978.
14 P. Schuster, G. Zundel and C. Sanderfy, *The Hydrogen Bond II, Structure and Spectroscopy*, North Holland Publishing Co., Amsterdam, 1976, ch. 8.
15 M. E. Brown, D. Dollimore and A. K. Galwey, *Comprehensive Chemical Kinetics*, eds. C. H. Bamford and C. J. Tipper, Elsevier, Amsterdam, 1980, vol. 22, p. 220.
16 H. J. Borchardt and F. Daniels, *J. Am. Chem. Soc.*, 1957, **79**, 41.

Paper 5/00568J
Received 31*st January* 1995
Accepted 1*st March* 1995